Microchim Acta (2011) 173:149–156
DOI 10.1007/s00604-010-0537-4

ORIGINAL PAPER

Synthesis of p-aminothiophenol-embedded gold/silver core-shell nanostructures as novel SERS tags for biosensing applications

Zhihui Luo · Kun Chen · Donglian Lu · Heyou Han · Mingqiang Zou

Received: 16 September 2010 / Accepted: 19 December 2010 / Published online: 8 January 2011

Abstract We describe a novel surface-enhanced Raman scattering (SERS) tag that is based on Au/Ag core-shell nanostructures embedded with p-aminothiophenol. The Au/Ag core-shell sandwich nanostructures demonstrate bright and dark stripe structure and possess very strong SERS activity. Under optimum conditions, the maximum SERS signal was obtained with a 10 nm thick Ag nanoshell, and the enhancement factor is 3.4×10^4 at 1077 cm^{-1}. After conjugation to the antibody of muramidase releasing protein (MRP), the Au/Ag core-shell nanostructures were successfully applied to an SERS-based detection scheme for MRP based on a sandwich type of immunoassay.

Keywords Au/Ag core-shell nanostructures · Surface enhanced Raman scattering · Biosensing · Immunoassay · Muramidase released protein

Introduction

Core-shell nanostructures (CS NSs) have attracted much attention in recent years due to their excellent stability, controllability, catalytic and optical characteristics [1–4]. Among them, noble metal CS NSs have been proven to be good candidate for biosensing, especially in SERS-based immunoanalysis [5–7]. SERS, a rapid, sensitive, nondestructive detection technology, has been widely applied in bioanalysis in recent 30 years [8–12]. It not only provides abundant vibrational information of the biomolecular system, but also serves as a quantitative technique for the detection of biomolecules, pathogens, and disease markers [13, 14]. At present, a key challenge to the wide bioapplications of SERS using noble metal nanoparticles (NPs) as substrates is to design reasonable, reproducible and highly active structures for analytical applications. Most of the solution-phase experiments in SERS are carried out using either Ag or Au NPs, it is well known that Au NPs are good candidate for bioapplications due to their excellent biocompatibility and low cyctotoxicity, while they only perform moderate enhancement to SERS detection. In contrast, the SERS activity of Ag NPs is higher than that of Au NPs, but they are unstable in solution and tend to aggregate [15]. Up to now, bimetal Au/Ag or Ag/Au CS NSs have been intensively investigated for their activity as SERS substrates [16–20]. For example, Cui et al. studied the SERS activity of the bimetallic Ag/Au CS NSs with some pinholes on the surface, and found that their SERS activity depended on the molar ratio of Ag to Au. Furthermore, the Ag/Au CS NSs were then labeled with monoclonal antibodies and SERS probes and successfully used for immunoassay analysis [6]. Most recently, Choo and co-workers have developed rhodamine 6 G embedded gold-silver CS NSs with highly sensitive SERS and demonstrated their use in biological imaging of HEK293 cells expressing PLC 1 cancer markers [15].

Streptococcus suis type2 (SS2) is an important infectious disease of human and swine, it not only contributes substantially to economic losses in the swine industry worldwide, but also endangers human health. *Muramidase*

Z. Luo · K. Chen · D. Lu · H. Han (✉)
College of Science, State Key Laboratory of Agricultural Microbiology, Huazhong Agricultural University, Wuhan 430070, People's Republic of China
e-mail: hyhan@mail.hzau.edu.cn

M. Zou
e-mail: mingqiangz@sina.com

M. Zou (✉)
Chinese Academy of Inspection and Quarantine, Beijing 100025, People's Republic of China

released protein (MRP) is one of the significant biomarker protein of SS2 [21]. The detection of MRP can provide potentially valuable information for diagnosis of SS2. Currently, many microbiological and molecular biological methods have been applied to test MRP including polymerase chain reaction, enzyme-linked immunosorbent assay and immunofluorescence assay based on quantum dot probe [22, 23]. However, these methods required specialized laboratory equipment, multistep sample handling and exhaustive separation procedures. Therefore, it still remains a great challenge to develop a rapid and sensitive method for the detection of MRP. To the best of our knowledge, few SERS-based immunoassay techniques have been reported to detect MRP using Au/Ag CS NSs.

In this study, we prepared pATP embedded Au/Ag CS NSs in aqueous solutions, and then the SERS activity of as-prepared CS NSs was systematic investigated. The results showed that the SERS activity were effectively tuned by modulating the thickness of Ag nanoshell, and the maximum enhancement factor (EF) reached 3.4×10^4 at 1077 cm^{-1} with 10 nm thickness of Ag nanoshell. More importantly, a novel SERS-immunoassay was carried out for the detection of MRP using as prepared nanostructures as SERS substrate (Scheme 1), the results demonstrated highly sensitive detection of MRP and the developed method has potentials for SERS based detection of other biomarker proteins.

Experimental

Materials

p-Aminothiophenol (pATP) was obtained from Acros Organics Inc. (Belgian. http://www.acros.be). Hydrogen tetrachloroaurate, silver nitrate, ascorbic acid, and trisodium citrate were purchased from Sinopharm Chemical Reagent Co. (Shanghai, China. http://sinoreagent.cn.alibaba.com). MRP, MRP antibody and serum sample of infected pigs were provided by State Key Laboratory of Agricultural Microbiology, Huazhong Agricultural University, China. Other chemicals were all of reagent grade and used without further purification. Ultrapure water was used throughout the experiments.

Instruments

SERS was obtained using invia Raman spectrometer (Renishaw, UK. http://www.renishaw.com) equipped with

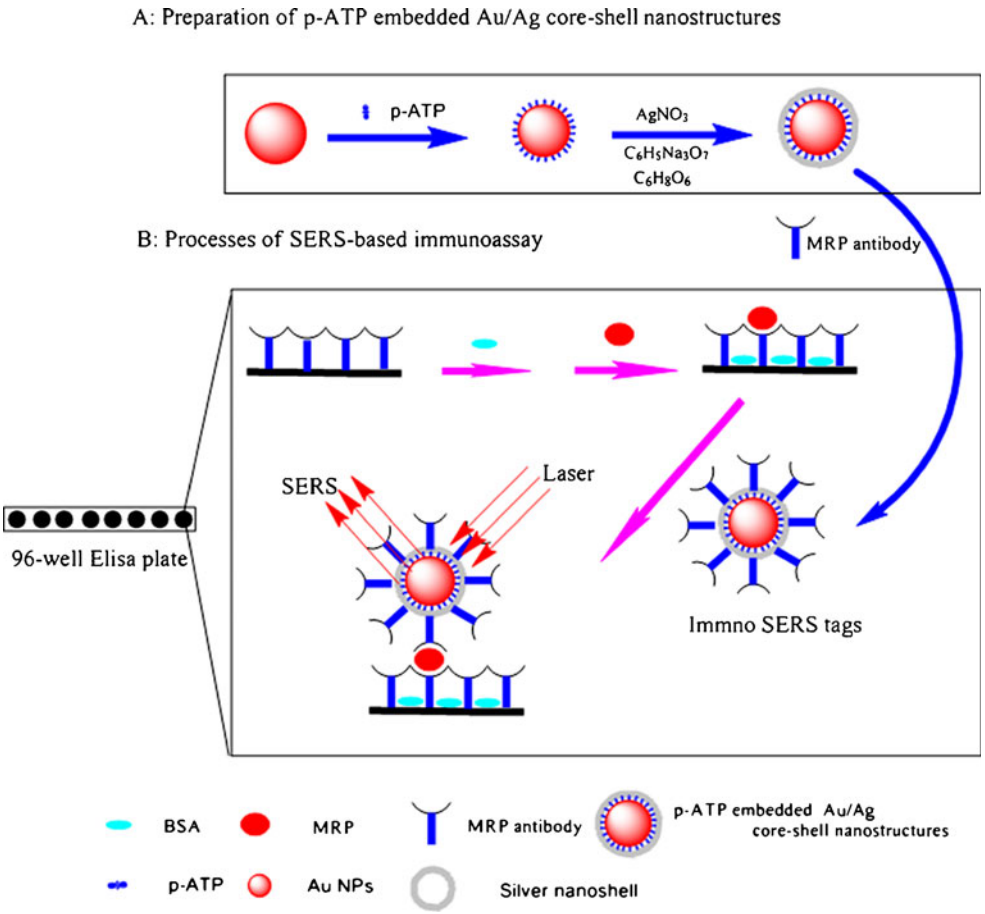

Scheme 1 Preparation processes of SERS-based immunoassay with pATP embedded Au/Ag CS NSs

cofocusing microscope (Leica, German. http://www.leica-microsystems.com). A He-Ne laser (633 nm) was used as the excitation source with a laser power of approximately 2 mW on the sample, and a 50×long-local-length objective microscope was used to focus a laser spot (2 μm) on the sample. The band of a silicon wafer at 520 cm^{-1} was used to calibrate the spectrometer. The SERS spectra were obtained with the exposure time of 10 s and one time accumulation. The UV–vis absorption spectra were acquired using a Thermo Nicolet 300 UV–vis spectrometer (Thermo Nicolet, the United Stated. http://www.thermoscientific.com/). Transmission electron microscopy (TEM) images were taken from Tecnai G20 microscopy (FEI, Czech. http://www.fei.com).

Preparation of pATP embedded Au/Ag CS NSs

Firstly, the initial Au NPs were obtained by following the modified recipes of Frens [24]. 1.05 mL of trisodium citrate solution (1% w/v) was added into the boiling $HAuCl_4$ solution (100 mL, 0.24 mmol·L^{-1}) with vigorous stirring, and the mixture was then kept boiling for 10–12 min, after that mauve mixture was allowed to cool to room temperature under continuous stirring. pATP embedded Au/Ag CS NSs were prepared using a seed-mediated growth method. In a typical process, 60 μL of 1.1×10^{-3} mol·L^{-1} pATP in ethanol was added to 30 mL of prepared Au NPs under vigorous stirring, the mixed solution turned purple from mauve immediately, and the reaction was kept for 30 min at room temperature. The coated Au NPs were then separated from solution by centrifugation at 5000 rpm for 18 min. The unconjugated pATP were removed and the sediment was resuspended with 10 mL of ultrapure water. The purification was repeated for one more time. Then the pH value of the obtained resuspended solution was adjusted to 5.5 with 0.1 mol L^{-1} HCl. Subsequently, 1 mL prepared Au-pATP solution and 100 μL 1% trisodium citrate were dispersed in 2.5 mL water, then a desired volume of 10 mmol L^{-1} $AgNO_3$ was added under continuous stirring. Afterward, 100 μL of 0.1 mol L^{-1} ascorbic acid was added to the above solution, after 30 min stirring, the pATP embedded Au/Ag CS NSs were purified by centrifugation (4000 rpm, 20 min, 2 times).

Preparation of immuno-pATP embedded Au/Ag CS NSs

100 μL of 0.5 mg mL^{-1} MRP antibody was slowly added to 1.0 mL pATP embedded Au/Ag CS NSs solution to form the conjugates through electrostatic and hydrophobic interactions [25, 26]. After reaction for 2 h at room temperature, the solution was centrifuged at 8000 rpm for 12 min, and the supernatant containing uncombined antibody was discarded. The precipitate were resuspended in 1 mL of buffer solution (PBS: pH=7.2, 0.85% (w/v) NaCl, 0.03% (w/v) NaH_2PO_4, 0.22% (w/v) Na_2HPO_4).

Immobilization of MRP antibody on 96-well Elisa plate

The MRP antibody (0.2 mg mL^{-1}) was dropped to the 96-well Elisa plate with 100 μL per well, and incubated for 12 h at 4 °C, then the 96-well Elisa plate was washed with rinsing solution (pH=7.2, 0.85% (w/v) NaCl, 0.03% (w/v) NaH_2PO_4, 0.22% (w/v) Na_2HPO_4, 0.05% (v/v) Tween-80) to remove the excessive antibody and then dried with nitrogen. Finally, 2% bovine serum albumin in PBS was used to block active sites between antibody molecules to avoid nonspecific absorption. The 96-well Elisa plate was washed three times by rinsing solution to remove residual BSA.

Immunoassay protocol

MRP was diluted with PBS buffer to obtain a serial of concentrations. For each MRP antibody immobilized well, 100 μL MRP solution was added and incubated at 37 °C for 60 min. Rinsed three times with rinsing water, each well was further incubated with 100 μL of SERS tags for 1.5 h at room temperature. After washing three times by rinsing water solution to remove unbound SERS tags, the substrate was dried with nitrogen before SERS measurement.

Results and discussion

Characterization of pATP embedded Au/Ag CS NSs

Figure 1 shows the evolution of UV–vis absorption spectra and the digital pictures of pATP embedded Au/Ag CS NSs with different thickness of silver nanoshell. The results indicated that Au NPs exhibited surface plasmon absorbance peak at around 534 nm (Fig. 1Aa). After addition of pATP solution, this peak redshifted to 548 nm (Fig. 1Ab), which indicated pATP molecules had absorbed to the surface of Au NPs through the S–Au bond [27]. It is well known that the red shift of the SPR peak corresponds to the increase of particle's size [28]. When the pATP molecules were added into the citrate-stabilized Au NPs, it was instead of citrate and absorbed covalently to the surface of Au NPs through the S–Au bond. Low concentration of pATP affects the surface charges slightly, and the interparticle distances are substantially greater than the average particle diameter. As a result, the SPR peak is slightly redshifted. In contrast, too many pATP molecules may result in seriously reduced surface charges and shortened interparticle distances of Au NPs, certain aggregation of Au NPs is observed and a new SPR peak at longer wavelengths is appear [29–31]. In the experiment, the dispersed pATP-Au NPs were obtained with a little amount of pATP. When silver nitrate and ascorbic acid were added, a new absorption peak of the solution were observed at about 529 nm, the blueshifted

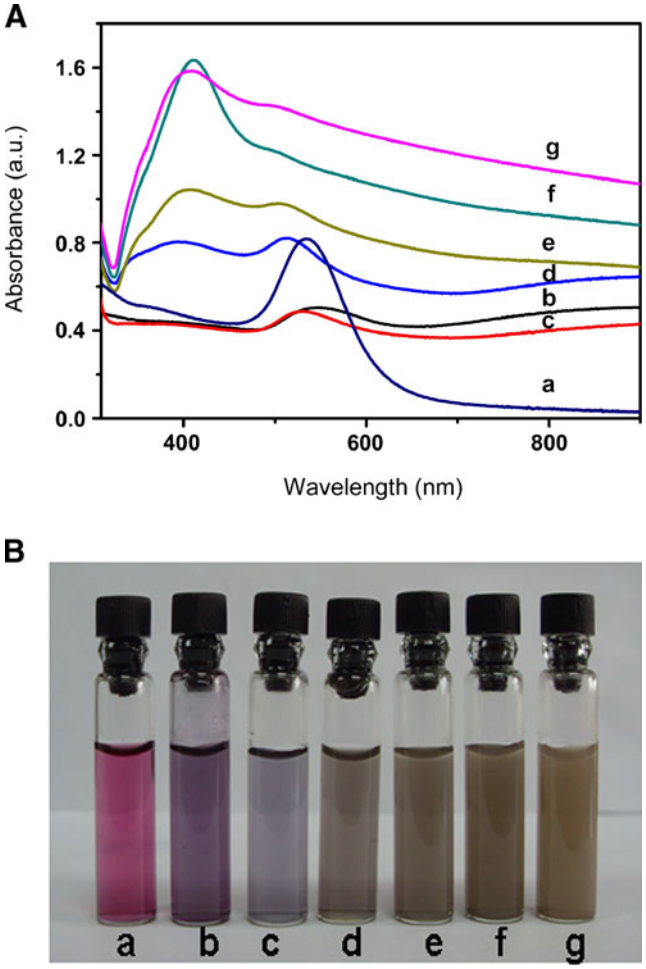

Fig. 1 The Evolution of UV–vis absorption spectra and the digital pictures of pATP embedded Au/Ag CS NSs after adding different volume of $AgNO_3$ (c–g): **a** AuNPs, **b** AuNPs-pATP, **c** 20, **d** 50, **e** 100, **f** 200 and **g** 300 μL, 10 mmol L^{-1} $AgNO_3$

wavelength suggested that Au/Ag CS NSs were formed [17]. However, with the increasing $AgNO_3$ amount, an absorption band appeared at about 400 nm, which were exclusively attributed to plasmon resonance of Ag NPs. With the increase of Ag nanoshell thickness, the intensity of the maximum absorption peak became stronger correspondingly. At the same time, the characteristic absorption peak of Au NPs disappeared gradually, as shown in Fig. 1A(c–g). The UV–vis absorption spectra inferred that the negatively charged Ag NPs assembled onto the surface of Au NPs with amino-groups of pATP through electrostatic force, thus the sandwich structure of pATP embedded Au/Ag CS NSs with different thickness of silver nanoshell were prepared.

TEM was employed to investigate the morphology of the obtained NSs. As revealed in Fig. 2, the average size of Au NPs was about 50 nm (Fig. 2a), with the increasing amount of $AgNO_3$, the average size of pATP embedded Au/Ag CS NSs ranged approximately from 54 nm to 86 nm (Fig. 2(b–f)). This observation was consistent with the results of UV–vis absorption spectra. In addition, a bright and dark stripe structure of nanostructures was observed in Fig. 2(b–f), which further confirmed the formation of Au/Ag CS NSs, and these results were similar to the previous reports by Rivas et al. [32]. From the TEM of the single NPs (Fig. 2), the silver nanoshell on the Au/Ag CS NSs was thickened from incomplete coverage into complete surface coverage as the silver fraction rose.

Figure 3 shows the SERS spectra of as-prepared pATP embedded Au/Ag CS NSs and AuNPs-pATP. It is obviously observed that SERS intensity of pATP embedded Au/Ag CS NSs were stronger than that of Au NPs-pATP. Moreover, the derived molecular spectrum information of pATP embedded CS NSs was rich, while SERS of AuNPs-pATP can not be observed, which indicated the superiority of as prepared sandwich nanostructures. The observed Raman vibration bands at 1585, 1433, 1391 and 1140 cm^{-1} can be attributed to b_2 modes of pATP and the band at 1077 cm^{-1}, 1185 cm^{-1} corresponds to a_2 modes of pATP according to the literatures [33–35]. The localized electromagnetic field enhancement as well as charge transfer in as prepared sandwich structure materials were probably responsible for the above observation [16, 19, 34, 36, 37]. Furthermore, we found that the SERS signal of pATP embedded Au/Ag CS NSs was dependent on the thickness of Ag nanoshell. As shown in Fig. 3, as the thickness of silver nanoshell grew, the SERS signal of pATP embedded Au/Ag CS NSs first increased (Fig. 3(a–c)) and then declined (Fig. 3(c–e)). The shell thickness depended SERS activity can be explained by the plausible existence of pinholes or crevices in the silver nanoshell. The pinholes or crevices on the CS NSs can provide hot spots for electromagnetic field enhancement and thereby produce stronger SERS activity [6, 38, 39]. At the initial stage of silver deposition, the pinholes or crevices began to form, providing a higher SERS activity (Fig. 3a) than that of Au NPs. As the silver fraction rose, more pinholes or crevices were created, leading to a maximum SERS enhancement (Fig. 3c). Finally, the silver shell grew into a smooth and seamless surface and a reduced SERS activity was observed owning to the lack of hot spots (Fig. 3d) [40, 41].

The EF was estimated using the following equation [35, 42, 43]:

$$EF = (I_{SERS}/N_{ads})/(I_{bulk}/N_{bulk}).$$

Where I_{SERS} and I_{bulk} are the intensity in the SERS and normal Raman spectra, respectively. N_{bulk} is the molecule number of the solid pATP in the laser illumination volume, which can be determined via the laser spot and the penetration depth, N_{ads} is the total molecules number of pATP in the Au core and Ag shell NPs within the laser spot,

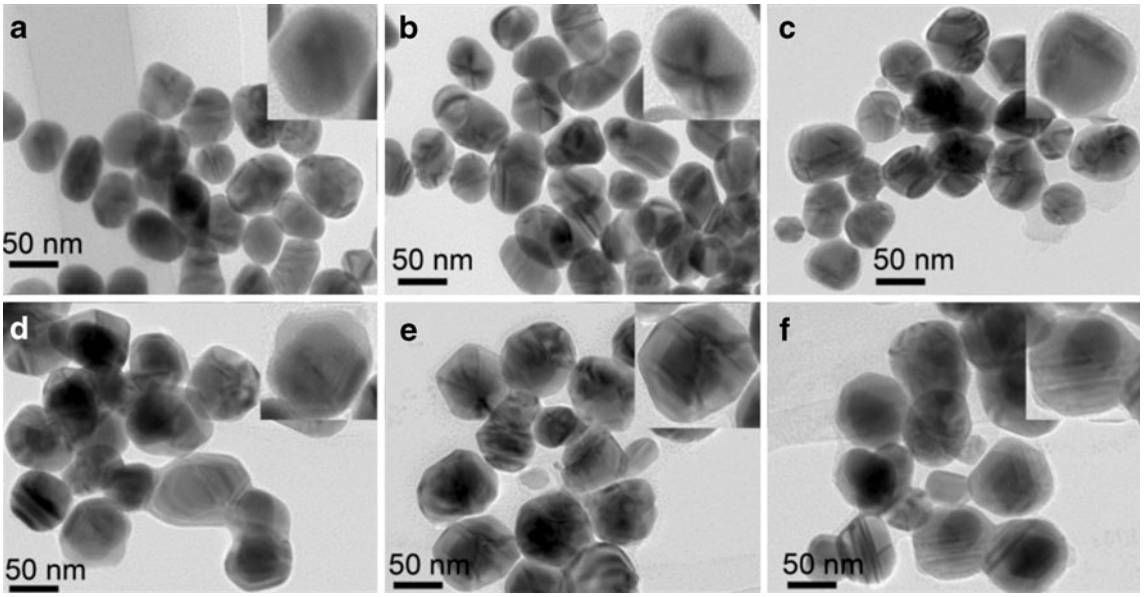

Fig. 2 TEM images of the obtained pATP embedded Au/Ag CS NSs after adding different volume of $AgNO_3$: **a** 0, **b** 20, **c** 50, **d** 100, **e** 200 and **f** 300 μL, 10 mmol L^{-1} $AgNO_3$

this value can be acquired through the equation [42]: $N_{ads} = N_d A_{laser} A_N/\sigma$. Where N_d is the number density of the Au core, A_{laser} is the area of the focal laser spot, and A_N is the area of one individual nanosphere and σ is the surface area occupied by one adsorbed pATP molecule, which was about 0.20 nm^2/molecule on the basis of the previous reports [33, 37, 44]. Under our experiment conditions, the intensity at 1077 cm^{-1} was selected to calculate the EF values, and the laser spot of 2 μm in diameter and the penetration depth of 15 μm by the focused laser beam are used [44, 45]. Here, N_{bulk} was calculated as 2.65×10^{11} considering N_d and A_N as 50 and 3.85×10^{-3} μm^2, respectively (from Fig. 2d), and A_{laser} as 2 μm. Finally, the EF value of pATP embedded Au/Ag CS NSs with 50 nm core diameter and 10 nm shell thickness was 3.4×10^4, indicating the excellent SERS-activity of as prepared pATP embedded Au/Ag CS NSs.

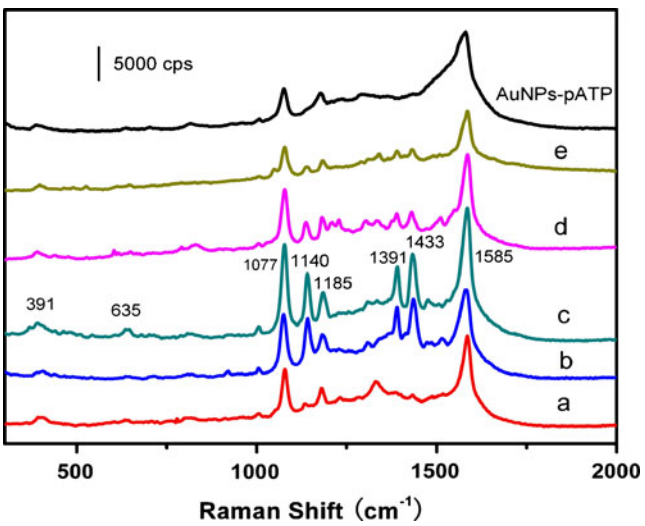

Fig. 3 SERS spectra of AuNPs-pATP and the obtained pATP embedded Au/Ag CS NSs after adding different volume of $AgNO_3$: **a** 20, **b** 50, **c** 100, **d** 200, **e** 300 μL, 10 mmol $L^{-1}AgNO_3$

SERS of immuno pATP embedded Au/Ag CS NSs

Figure 4 depicts the SERS spectra of antibody conjugated probes and 96-well Elisa plate substrate. The SERS signal of pATP between Au_{core} and Ag_{shell} was observed, which indicated such sandwich structural material was suitable for SERS studies. The observed Raman vibration bands were consisted with those of pATP embedded Au/Ag CS NSs. The signal may be attributed to the electromagnetic enhancement as well as the charge transfer in metal-molecular-metal sandwich structure [36, 37]. The SERS spectra at 1000, 1300 and 1600 cm^{-1} were observed when the 96-well Elisa plate was used in the experiment, while the signal of pATP was not influenced by those peaks.

SERS detection of MRP

To verify the feasible application of pATP embedded Au/Ag CS NSs, the immunoassay experiment was carried out for detection of MRP. In our work, the 96-well Elisa plate was used as a substrate to capture MRP antibody, while antibody conjugated NPs served as SERS nanoprobes. The sandwich structure complex was formed through antigen-antibody immunoreaction, as shown in Scheme 1. Figure 5 displays SERS spectra of the immune complexes in the presence of different concentrations of MRP. The

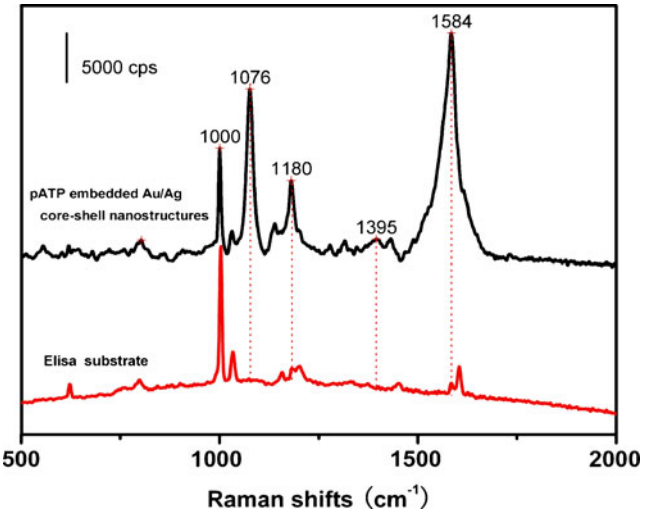

Fig. 4 SERS spectra of Elisa plate substrate and immuno-pATP embedded Au/Ag CS NSs

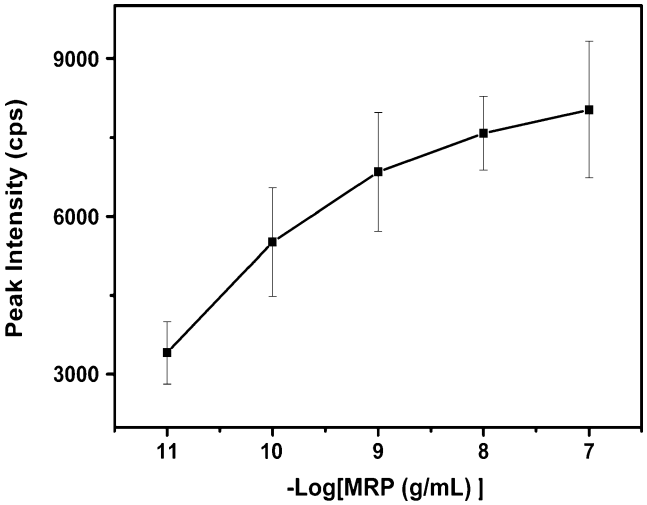

Fig. 6 The dose–response plots of the SERS-based immunoassay for MRP detection. Each data point represents average of 5 measurements (each *error bar* indicates the standard deviation)

spectra with two feature peaks at 1077 cm^{-1} and 1584 cm^{-1} were consistent with the signals of antibody conjugated probes. In addition, the blank spectra were obtained by replacing the MRP with BSA (10^{-6} mol·L^{-1}) to check the nonspecific absorption. Several peaks were observed from Fig. 5 (red curve), but they did not interfere with the peak at 1077 cm^{-1}. Therefore, the intensity of the peak at 1077 cm^{-1} was employed to quantify the MRP. Figure 6 shows the relationship between the intensity of signals at 1077 cm^{-1} and the concentration of MRP, it can be seen that the intensity of the peak at 1077 cm^{-1} was supposedly proportional to the concentration of MRP from 0.01 to 10 ng·mL^{-1} with the correlation coefficient (R^2) of 0.9534 (n=5). The linear regression equation was y=−1384x+ 18986, and the detection limit of MRP was as low as 1 pg mL^{-1}.

In order to verify the validity and reliability of this method, we have applied the prepared immuno SERS tags to detect MRP from four spleen serums (S_1, S_2, S_3 and S_4) and 4 liver serums (L_1, L_2, L_3, L_4) of infected pigs. The results are shown in Fig. 7. Comparing to SERS intensity of MRP (10 ng mL^{-1}) at 1077 cm^{-1}, MRP in seven serum samples were detected. In a contrast experiment where eight clinical serum samples were examined, the positive rates of SERS detection and traditional plate count method were 87.5% and 75%, respectively, indicating a high accordance rate between the two methods. In addition, this method provides remarkable advantages in terms of high sensitivity and specificity in animal disease detection.

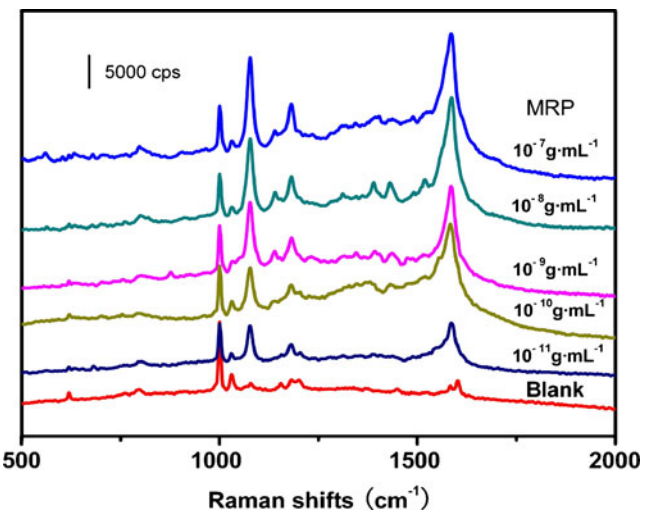

Fig. 5 SERS spectra of immuno-pATP embedded Au/Ag CS NSs with different concentration of MRP

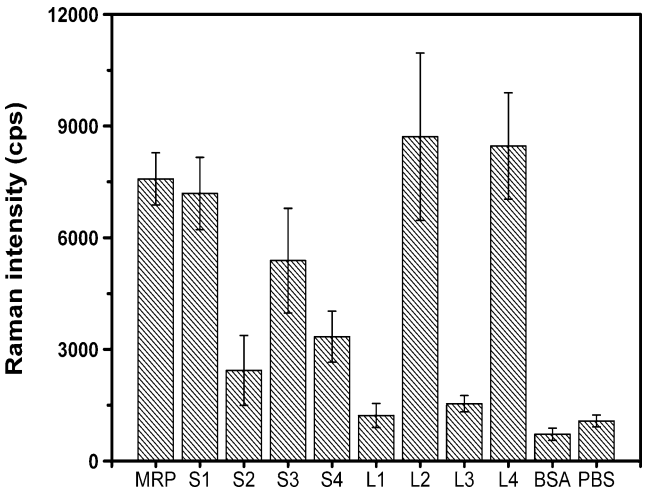

Fig. 7 Samples analysis of SERS assay: MRP (10 ng.mL^{-1}), S_1, S_2, S_3, S_4, L_1, L_2, L_3, L_4, BSA (10^{-6} mol·L^{-1}) and PBS, respectively

Conclusions

In summary, we took advantage of pATP embedded Au/Ag CS NSs to develop a novel biosensor for MRP. The synthesis of labeling molecular embedded Au/Ag CS NSs was facile and rapid. The prepared NPs with optimized shell thickness exhibited high SERS activity. Moreover, the SERS-immunoassay employing pATP embedded Au/Ag CS NSs as tags possessed high sensitivity toward MRP with a detection limit of 1 pg mL^{-1} and a high accordance rate with traditional method in real sample detection. This method can be further extended to practical and sensitive immunoassay of various biomolecules and diseases biomarkers.

Acknowledgements The authors gratefully acknowledge the support for this research by National Natural Science Foundation of China (20975042), the Program for academic pacesetter of Wuhan (200851430484), Nature Science foundation key project from Hubei Province of China (2008CDA080), International Science and Technology cooperation and Exchange Foundation (2008DFA40270) and the Fundamental Research Funds for the Central Universities of China (2009JC005).

References

1. Ung T, Liz-Marzán LM, Mulvaney P (1999) Redox catalysis using Ag@ SiO_2 colloids. J Phys Chem B 103:6770
2. Saunders A, Popov I, Banin U (2006) Synthesis of hybrid CdS-Au colloidal nanostructures. J Phys Chem B 110:25421
3. Kamata K, Lu Y, Xia Y (2003) Synthesis and characterization of monodispersed core-shell spherical colloids with movable cores. J Am Chem Soc 125:2384
4. Hu JW, Zhang Y, Li JF, Liu Z, Ren B, Sun SG, Tian ZQ, Lian T (2005) Synthesis of Au@Pd core-shell nanoparticles with controllable size and their application in surface-enhanced Raman spectroscopy. Chem Phys Lett 408:354
5. Xu W, Xu S, Ji X, Song B, Yuan H, Ma L, Bai Y (2005) Preparation of gold colloid monolayer by immunological identification. Colloids Surf B 40:169
6. Cui Y, Ren B, Yao JL, Gu RA, Tian ZQ (2006) Synthesis of Ag core Au shell bimetallic nanoparticles for immunoassay based on surface-enhanced Raman spectroscopy. J Phys Chem B 110:4002
7. Bao F, Yao JL, Gu RA (2009) Synthesis of magnetic Fe_2O_3/Au core/shell nanoparticles for bioseparation and immunoassay based on surface-enhanced Raman spectroscopy. Langmuir 25:10782
8. Shao M, Lu L, Wang H, Luo S, Ma D (2009) Microfabrication of a new sensor based on silver and silicon nanomaterials, and its application to the enrichment and detection of bovine serum albumin via surface-enhanced Raman scattering. Microchim Acta 164:157
9. Kang T, Yoo S, Yoon I, Lee S, Kim B (2010) Patterned multiplex pathogen DNA detection by Au particle-on-wire SERS sensor. Nano Lett 10:1189
10. Knauer M, Ivleva N, Liu X, Niessner R, Haisch C (2010) Surface-enhanced Raman scattering-based label-free microarray readout for the detection of microorganisms. Anal Chem 82:2766
11. Wang F, Shen H, Feng J, Yang H (2006) PNA-modified magnetic nanoparticles and their hybridization with single-stranded DNA target: surface enhanced Raman scatterings study. Microchim Acta 153:15
12. Porter MD, Lipert RJ, Siperko LM, Wang G, Narayanana R (2008) SERS as a bioassay platform: fundamentals, design, and applications. Chem Soc Rev 37:1001
13. Alvarez-Puebla R, Liz-Marzán L (2010) SERS-based diagnosis and biodetection. Small 6:604
14. Lin CC, Yang YM, Chen YF, Yang TS, Chang HC (2008) A new protein a assay based on raman reporter labeled immunogold nanoparticles. Biosens Bioelectron 24:178
15. Lee S, Kim S, Choo J, Shin SY, Lee YH, Choi HY, Ha S, Kang K, Oh CH (2007) Biological imaging of HEK293 cells expressing PLC 1 using surface-enhanced Raman microscopy. Anal Chem 79:916
16. Kahraman M, Aydm Ö, Çulha M (2009) Oligonucleotide-mediated Au-Ag core-shell nanoparticles. Plasmonics 4:293
17. Yang Y, Shi J, Kawamura G, Nogami M (2008) Preparation of Au-Ag, Ag-Au core-shell bimetallic nanoparticles for surface-enhanced Raman scattering. Scr Mater 58:862
18. Cao Y, Jin R, Mirkin C (2001) DNA-modified core-shell Ag/Au nanoparticles. J Am Chem Soc 123:7961
19. Huang Y, Yang Y, Chen Z, Li X, Nogami M (2008) Fabricating Au-Ag core-shell composite films for surface-enhanced Raman scattering. J Mater Sci 43:5390
20. Lim DK, Kim IJ, Nam JM (2008) DNA-embedded Au/Ag core-shell nanoparticles. Chem Commun 42:5312
21. Staats JJ, Feder I, Okwumabua O, Chengappa MM (1997) Streptococcus suis: past and present. Vet Res Commun 21:381
22. Chu CY, Shu SF, Huang JH, Hsu JP, Xue KR (2009) Rapid detection of streptococcus suis serotypes and virulent factors in southern taiwan by multiplex polymerase chain reaction. Taiwan Vet J 35:107
23. Wu HM, Han HY, Jin ML, Zhang AD (2009) A novel method to detect muramidase released protein (MRP) antigen of streptococcus sui serotype 2 based on CdSe/ZnS quantum dot probe. Acta Chimi Sin 67:1087
24. Frens G (1973) Controlled nucleation for regulation of particle-size in monodisperse gold suspensions. Nat Phys Sci 241:20
25. Duan C, Meyerhoff ME (1994) Separation-free sandwich enzyme immunoassays using microporous gold electrodes and self-assembled monolayer/immobilized capture antibodies. Anal Chem 66:1369
26. Yakovleva J, Davidsson R, Lobanova A, Bengtsson M, Eremin S, Laurell T, Emneus J (2002) Microfluidic enzyme immunoassay using silicon microchip with immobilized antibodies and chemiluminescence detection. Anal Chem 74:2994
27. Jang S, Park J, Shin S, Yoon C, Choi BK, Gong MS, Joo SW (2004) Adsorption of 4-biphenylmethanethiolate on different-sized gold nanoparticle surfaces. Langmuir 20:1922
28. Mie G (1908) Beiträge zur optik trüber medien, speziell kolloidaler metallösungen. Ann Phys 25:377
29. Thanh NTK, Rosenzweig Z (2002) Development of an aggregation-based immunoassay for anti-protein A using gold nanoparticles. Anal Chem 74:1624
30. Kreibig U, Genzel L (1985) Optical absorption of small metallic particles. Surf Sci 156:678
31. Song C, Wang Z, Zhang R, Yang J, Tan X, Cui Y (2009) Highly sensitive immunoassay based on raman reporter-labeled immuno-Au aggregates and SERS-active immune substrate. Biosens Bioelectron 25:826
32. Rivas L, Sanchez-Cortes S, Garcia-Ramos JV, Morcillo G (2000) Mixed silver/gold colloids: a study of their formation, morphology, and surface-enhanced Raman activity. Langmuir 16:9722

33. Wang Y, Chen H, Dong S, Wang E (2006) Surface enhanced Raman scattering of p-aminothiophenol self-assembled monolayers in sandwich structure fabricated on glass. J Chem Phys 124:074709
34. Zhou Q, Li X, Fan Q, Zhang X, Zheng J (2006) Charge transfer between metal nanoparticles interconnected with a functionalized molecule probed by surface-enhanced Raman spectroscopy. Angew Chem Int Ed 45:3970
35. Osawa M, Matsuda N, Yoshii K, Uchida I (1994) Charge transfer resonance Raman process in surface-enhanced Raman scattering from p-aminothiophenol adsorbed on silver: Herzberg-teller contribution. J Phys Chem 98:12702
36. Wang Y, Zou X, Ren W, Wang W, Wang E (2007) Effect of silver nanoplates on Raman spectra of p-aminothiophenol assembled on smooth macroscopic gold and silver surface. J Phys Chem C 111:3259
37. Kim K, Yoon JK (2005) Raman scattering of 4-aminobenzenethiol sandwiched between Ag/Au nanoparticle and macroscopically smooth Au substrate. J Phys Chem B 109:20731
38. Hao E, Li S, Bailey RC, Zou S, Schatz GC, Hupp JT (2004) Optical properties of metal nanoshells. J Phys Chem B 108:1224
39. Kumar GVP, Shruthi S, Vibha B, Reddy B, Kundu T, Narayana C (2007) Hot spots in Ag core-Au shell nanoparticles potent for surface-enhanced raman scattering studies of biomolecules. J Phys Chem C 111:4388–4392
40. Zhang P, Guo Y (2009) Surface-enhanced raman scattering inside metal nanoshells. J Am Chem Soc 131:3808
41. Jiang Y, Wang A, Tian ZQ, Otto A (2009) Is it possible to observe surface-enhanced raman scattering from buried molecules? J Phys Chem C 113:5526
42. Orendorff CJ, Gole A, Sau TK, Murphy CJ (2005) Surface-enhanced Raman spectroscopy of self-assembled monolayers: sandwich architecture and nanoparticle shape dependence. Anal Chem 77:3261
43. Ren B, Lin XF, Yang ZL, Liu GK, Aroca RF, Mao BW, Tian ZQ (2003) Surface-enhanced Raman scattering in the ultraviolet spectral region: UV-SERS on rhodium and ruthenium electrodes. J Am Chem Soc 125:9598
44. Gole A, Sainkar SR, Sastry M (2000) Electrostatically controlled organization of carboxylic acid derivatized colloidal silver particles on amine-terminated self-assembled monolayers. Chem Mater 12:1234
45. Zhang DF, Niu LY, Jiang L, Yin PG, Sun LD, Zhang H, Zhang R, Guo L, Yan CH (2008) Branched gold nanochains facilitated by polyvinylpyrrolidone and their SERS effects on p-aminothiophenol. J Phys Chem C 112:16011